Chinese Chemical Letters 35 (2024) 108432

Contents lists available at ScienceDirect

Chinese Chemical Letters

journal homepage: www.elsevier.com/locate/cclet

# Advances in selective catalytic oxidation of ammonia ($NH_3$-SCO): A review of catalyst structure-activity relationship and design principles

Zhao Li[a], Chunxue Wang[a], Junjun Qiu[a], Yixing Ma[a,b], Chi Wang[c], Xin Sun[a,b], Kai Li[a,b,*], Ping Ning[a,b], Fei Wang[a,b,*]

[a] Faculty of Environmental Science and Engineering, Kunming University of Science and Technology, Kunming 650500, China
[b] National-Regional Engineering Center for Recovery of Waste Gases from Metallurgical and Chemical Industries, Kunming 650500, China
[c] Faculty of Chemical Engineering, Kunming University of Science and Technology, Kunming 650500, China

ARTICLE INFO

*Article history:*
Received 29 September 2022
Revised 9 March 2023
Accepted 4 April 2023
Available online 6 April 2023

*Keywords:*
Ammonia
Selective catalytic oxidation
Active metals and supports
Influence of gas composition
Reaction mechanism
Catalyst structure-activity relationship

ABSTRACT

$NH_3$ in ambient air directly leads to an increase in the aerosol content in the air. These substances lead to the formation of haze to various environmental problems after atmospheric circulation and diffusion. Controlling $NH_3$ emissions caused by ammonia escaping from mobile and industrial sources can effectively reduce the $NH_3$ content in ambient air. Among the various $NH_3$ removal methods, the selective catalytic oxygen method ($NH_3$-SCO) is committed to oxidizing $NH_3$ to environmentally harmless $H_2O$ and $N_2$; therefore, it is the most valuable and ideal ammonia removal method. In this review, the characteristics of loaded and core-shell catalysts in $NH_3$-SCO have been reviewed in the context of catalyst structure-activity relationships, and the $H_2O$ resistance and $SO_2$ resistance of the catalysts are discussed in the context of practical application conditions. Then the effects of the valence state of the active center, oxygen species on the catalyst surface, dispersion of the active center and acidic sites on the catalyst performance are discussed comprehensively. Finally, the shortcomings of the existing catalysts are summarized and the catalyst development is discussed based on the existing studies.



## 1. Introduction

$NH_3$ is a colorless gas that is widely used in various industries. However, with industrial development, an increasing amount of unusable $NH_3$ is discharged into the atmosphere. Approximately 80% of the total $NH_3$ in the atmosphere is emitted by human beings [1]. These $NH_3$ emissions to the environment mainly come from agriculture and animal husbandry (volatilization of animal manure and synthetic fertilizers), industrial and motor vehicle exhaust (combustion of fossil fuels, nitrate manufacturing and $NH_3$ escape in the selective catalytic reduction [SCR] process). In addition, with the continuous development of the economy and increasingly strict emission standards of pollutants, the SCR process must add more $NH_3$ as a reducing agent to discharge lower concentrations of $NO_x$. When a small amount of $NO_x$ is discharged, more $NH_3$ escapes into the atmosphere [2]. In recent years, owing to the use of SCR catalytic converters in diesel vehicles, moving $NH_3$ emissions have significantly increased [3,4]. In addition, the use of concrete admixtures, wood panels and widely used interior decoration materials in the construction industry, urban sewage systems and urban garbage will cause $NH_3$ emissions to a certain extent [5–7].

Ammonia has a pungent odor and high concentrations stimulate the respiratory tract, lung mucosa, conjunctiva and cornea to damage the respiratory system [8,9]. In addition, a higher $NH_3$ concentration in the atmosphere often leads to a decrease in the photosynthetic rate of plants. When $NH_3$ migrates to the water environment, it easily leads to eutrophication of the water quality and soil acidification [10–14]. When $NH_3$ is discharged into the atmosphere, it reacts rapidly with acid gases in the environment and exists in the form of secondary inorganic aerosols such as ammonium nitrate and ammonium sulfate. These aerosols are important precursors of PM2.5 in the atmospheric environment [1,15,16]. These secondary inorganic aerosols further react with carbonyl compounds to produce nitrogen-containing organic compounds, which significantly increases the NOC content in the air environment. These multistage products produced by $NH_3$ are also one of the main causes of haze [17–21]. Aerosols formed by nitrate and sulfate in the air also have an important impact on global radiation. As the core of haze and water vapor condensation in clouds,

* Corresponding authors.
*E-mail addresses:* likaikmust@163.com (K. Li), wangfei@kust.edu.cn (F. Wang).

https://doi.org/10.1016/j.cclet.2023.108432
1001-8417/

they can indirectly increase the lifespan of clouds [1]. When $NH_3$ in the atmosphere is oxidized, $NO_x$ from $NH_3$ oxidation cause serious photochemical pollution. Moreover, $N_2O$ is a powerful greenhouse gas.

In conclusion, $NH_3$ acts as an important N compound and greatly affects the reaction and migration of N in the atmosphere. $NH_3$ participates in the atmospheric N cycle, which affects climate change, human health and ecosystem stability. Therefore, it is necessary to control and reduce $NH_3$ anthropogenic emissions to protect the ecological environment and to further develop the economy.

## 2. $NH_3$ purification method

According to the difference in the conditions of the ammonia-containing waste gas to be eliminated, there are various treatment methods, such as adsorption, absorption, biofiltration, catalytic combustion, catalytic oxidation, photocatalysis and electrocatalysis, *etc.* [22–25]. Considering the technical and/or economic limitations of treatment technologies in industry and transportation, selective catalytic oxidation of ammonia ($NH_3$-SCO) into nitrogen and water is a highly promising process to reduce ammonia emissions.

## 3. $NH_3$-SCO catalyst

Supported catalysts and core-shell catalysts composed of stable metal oxides or mixtures and active sites have been widely studied because the $NH_3$-SCO reaction is an O-containing thermal-catalytic reaction, which leads to the lack of advantages of C-based materials and unstable MOF materials. Common supports include $Al_2O_3$, SSZ-13, SAPO-34, ZSM-5, $TiO_2$, $ZrO_2$, $Ce_xZr_yO_2$ (x and y represent the mass ratio of elements) and other materials. The support generally has no catalytic activity, however, its excellent surface structure is conducive to the dispersion of the active metal, and the construction of unique metal-support interactions improves the intrinsic activity of the catalyst [26–28]. However, the focus of core-shell catalysts is not here; the main purpose is to prevent $H_2O$ or $SO_2$ from contacting active metals through a stable outer shell structure to prevent active center poisoning.

### 3.1. Supported catalyst

Supported catalysts are typically prepared by combining a support with an active metal. The difference between the support and the active component leads to a difference in the interaction between them, therefore, the activity of the prepared catalyst is also different [29–31]. For supported catalysts, stable oxides or materials with a certain framework structure are usually selected as supports. Currently, $Al_2O_3$, $TiO_2$ and various zeolites are widely used as supports. There are many electronic defects on $TiO_2$, which lead to a strong metal-support interaction (SMSI). The structures of $Al_2O_3$ and zeolites are stable and difficult to reduce. Generally, the SMSI between various atoms is weak on $Al_2O_3$ and zeolite, which also leads to high stability of the two supports [29,32]. Although some supports have a certain activity for $NH_3$-SCO, the active metal anchored on the support provides the main active site for the decomposition, adsorption and oxidation of $NH_3$.

The active center of a catalyst is typically composed of noble or transition metals. Noble metals, as active components, generally enable catalysts to have stronger oxidation performance, whereas cheap metals have lower catalytic activity than that of noble metals. However, it is easier to commercialize catalysts loaded with inexpensive metals because of the low cost.

#### 3.1.1. Cheap metals

Transition metals are relatively inexpensive; therefore, they are widely used as active materials. The catalytic activity exhibited by different combinations of active metal and support is irregular; therefore, it cannot be assumed that a certain catalyst has high catalytic activity, and the high catalytic activity is considered to be caused by the active metal. According to our previous research and current experiments [33,34], as an active substance, Ag has excellent $NH_3$ activity and higher $NH_3$ conversion than Fe (Figs. 1a, b). However, when using $\beta$-SMAD to support Fe, even under 325 °C reaction conditions, it shows 100% $NH_3$ conversion and 99.54% $N_2$ selectivity at GHSV of 50,000 $h^{-1}$ (Figs. 1c, d) [2]. Thus, this result is only for the comparison of the active metal components on nano-$Al_2O_3$. For different supports, the SMSI and support are different, therefore, it is impossible to judge the activity of the catalyst according to the activity of the metal and the experimental data is shown in Figs. 1e–g [35].

Moreover, as the mass of active components loaded on the support increased, the $NH_3$-SCO activity of the catalyst also increased accordingly. However, this does not mean that the catalyst activity also increases indefinitely when the active components increase indefinitely. When a large number of active metals are loaded, the active metal aggregates on the surface of the support, which blocks the pore channel of the catalyst and reduces the specific surface area of the catalyst, leading to a decrease in the catalytic activity. Although cheap metals have a certain degree $NH_3$-SCO activity, their redox performance of cheap metals as active centers on supported catalysts is lower than that of noble metals [36,37]. Notably, the temperature window of the iron-based catalyst $T_{100}$ is typically higher (approximately 400 °C or higher) [38–41]. In addition, Cu-based catalyst research has also been widely studied, with a $T_{100}$ of approximately 300 °C [33,40,42–45].

#### 3.1.2. Noble metals

Noble metals have stronger redox properties than inexpensive metals, and catalysts loaded with noble metals often have better catalytic activity. Pt, Ru, Pd, Rh, Au and Ag are the commonly used noble metals in $NH_3$-SCO. Noble metal, as the active center of the catalyst, can show high $NH_3$ oxidation activity even at low-temperatures. However, because of its strong oxidizing properties, it can easily cause excessive oxidation of $NH_3$, thereby generating by-products, such as $NO_x$ and $N_2O$ [46–49]. Shin *et al.* loaded Ru or Pt onto $TiO_2$ (Figs. 1h and i), and the results showed that Ru/$TiO_2$ can reach 90% at 250 °C, and the conversion rate of $NH_3$ was 30% higher than that of Pt/$TiO_2$ at this temperature. In addition, the $N_2$ selectivity of Pt/$TiO_2$ was only 40% below 60% of Ru/$TiO_2$ [50].

Existing studies have found that, on supported catalysts with precious metals as the active center, the selectivity for $N_2$ decreases with an increase in temperature, although the conversion rate of $NH_3$ will always increase with an increase in temperature (all catalysts of noble metals can achieve a 100% conversion rate at 350 °C). The $N_2$ selectivity began to decrease gradually at reaction temperatures above 200 °C, and the $N_2$ selectivity can reach 100% at temperatures below 200 °C. The yield of $N_2O$ first increases and then decreases with an increase in temperature, and the temperature is different when the yield reaches its peak value on different catalysts. In addition, $NO_x$ production increases with increasing temperature [46,51,52]. Notably, most of the noble metal catalysts currently used in the field of $NH_3$-SCO use noble metal nanoparticles as active centers (Fig. 2), which means that the loading of noble metals is frequently high (about 1 wt%). In other fields, the precious metal loading of most catalysts is only 0.2 wt% or lower [53–56]. Although noble metal catalysts exhibit good performance, there is no strategic significance to develop high-loaded noble metal nanoparticle catalysts when low-loaded single-atom catalysts are prevalent today.

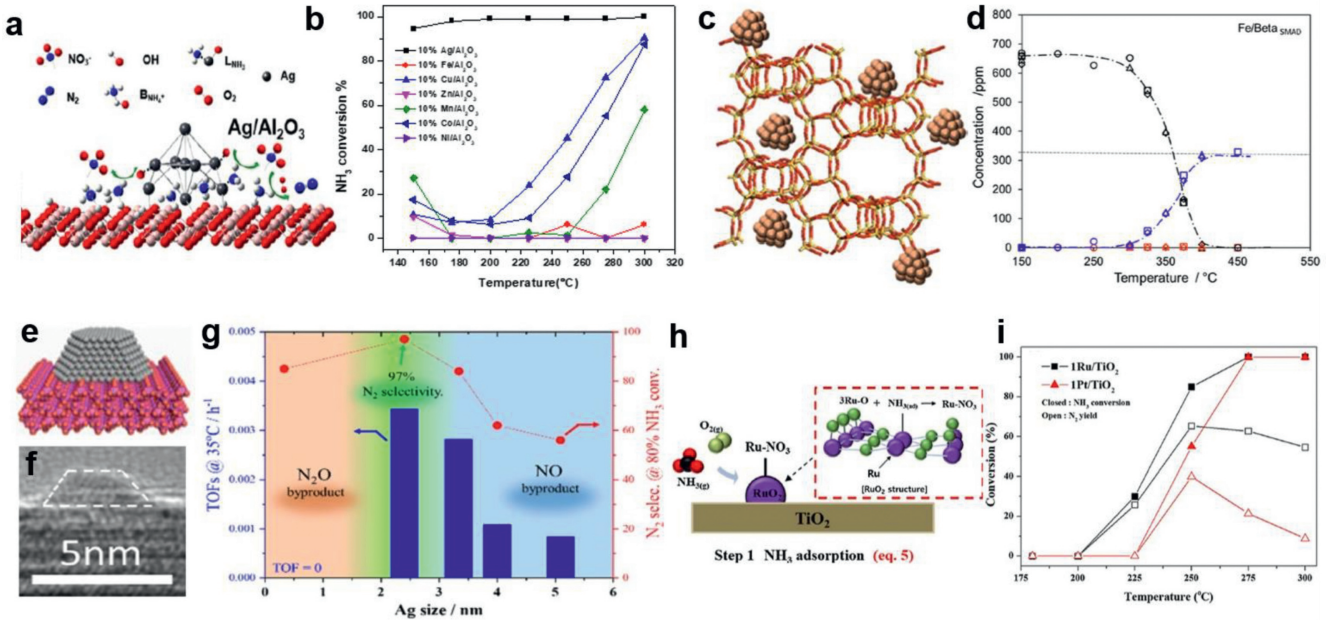


**Fig. 1.** Schematic structure and $NH_3$-SCO activity of a series of supported catalysts. (a, b) $Ag_{NPs}$ supported on $Al_2O_3$ and active test. (Reaction conditions: $NH_3 = 500$ ppm, $O_2 = 10$ vol%, GHSV = 28,000 $h^{-1}$). Copied with permission [34]. Copyright 2019, American Chemical Society. (c, d) Loading $Fe_{NPs}$ over beta zeolite and corresponding $NH_3$-SCO activity, concentration profiles of $NH_3$ (black markers), $N_2$ (blue markers), and $N_2O$ (red markers) (Reaction conditions: $NH_3 = 650$ ppm, $O_2 = 5$ vol%, GHSV = 50,000 $h^{-1}$). Copied with permission [2]. Copyright 2019, American Chemical Society. (e-g) TEM image, schematic structure and corresponding catalyst performance of 5 nm $Ag_{NPs}$ supported on $MnO_2$ (Reaction conditions: $NH_3 = 50$ ppm, $O_2 = 20$ vol%, GHSV = 40,000 $h^{-1}$). Copied with permission [35]. Copyright 2021, American Chemical Society. (h, i) RuO supported on $TiO_2$ and active test (Reaction conditions: $NH_3 = 500$ ppm, $O_2 = 10$ vol%, GHSV = 6,000 $h^{-1}$). Copied with permission [50]. Copyright 2020, Elsevier.

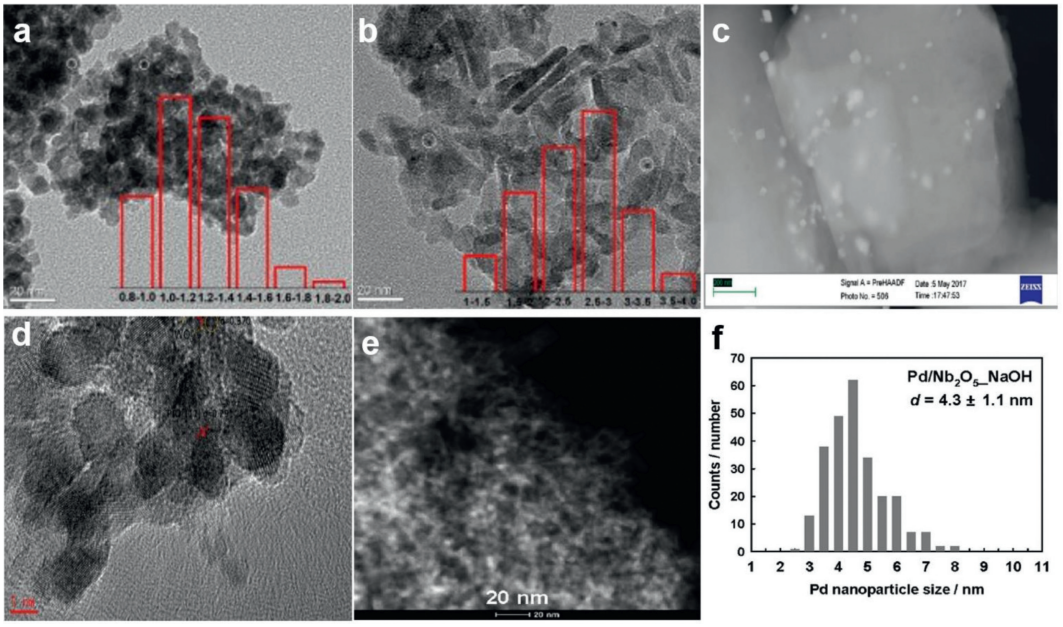


**Fig. 2.** TEM images of a series of supported noble metal catalysts applied to $NH_3$-SCO. (a) 1%Pt/$CeZrO_2$, (b) 1%Pt/$Al_2O_3$. Copied with permission [46]. Copyright 2019, American Chemical Society. (c) 1.5%Pt/ZSM-5. Copied with permission [51]. Copyright 2017, Elsevier. (d) 1.5%Pt-$WO_3$/$ZrO_2$. Copied with permission [55]. Copyright 2017, Elsevier. (e, f) 1%Pd/$Nb_2O_5$ and Pd particle size distribution. Copied with permission [56]. Copyright 2020, Elsevier.

### *3.1.3. Ag base catalyst*

Many researchers have focused on Ag to improve the activity and lessen the cost of catalysts. As an active metal, Ag can make the catalyst price close to that of cheap metal catalysts. It also has high catalytic activity, similar to that of noble metal catalysts. The catalyst prepared by loading Ag on nano-$Al_2O_3$ has high $NH_3$ activity, and, combined with other studies, it was found that Ag as an active component of $NH_3$ catalysis has high low-temperature activity and $N_2$ selectivity [57,58].

Ag-based catalysts show good activity in the $NH_3$-SCO reaction, whether back-supported on $SiO_2$, molecular sieves, $Al_2O_3$, or other supports. The $T_{100}$ of the catalyst with Ag loading between 5 wt% and 10 wt% was approximately 200 °C under the condition that the space velocity was >35,000 $h^{-1}$ [59–62]. Ag species are unique compared to other active metals. Multiple studies have shown that the O activation energy required for the O vacancy energy of active metal oxides is lower; however, the activity of Ag oxide itself is lower than that of $Ag^0$. Therefore, Ag species do not rely on

the O vacancies of oxides to lower the O activation energy barrier, but rely on the O activation ability of $Ag^0$ itself to promote $NH_3$-SCO [34,63]. Wang *et al.* loaded $Ag_{NPs}$ of different particle sizes on the $MnO_2$ surface. The results showed that $Ag_{NPs}$ with a size of 3 nm had the best activity in $NH_3$-SCO, which could reach 100% $NH_3$ conversion at 80 °C and with $N_2$ selectivity of 97% [35]. Nano-$Al_2O_3$ was loaded with 10% Ag to form $Ag_{NPs}$ with an average particle size of 3.7 nm, 100% $NH_3$ conversion, and 70% $N_2$ selectivity at 120 °C, but a GHSV of 120,000 $h^{-1}$ [57].

This was demonstrated in a previous study where 10% Ag/$Al_2O_3$ was reduced by $H_2$ at 400 °C, the $Ag_2O$ species were converted to $Ag^0$ with an average particle size of 5.4 nm, and the $T_{100}$ was reduced from 160 °C to 120 °C [34]. In addition, because Ag atoms are anchored to hydroxyl groups, the reduction treatment will agglomerate Ag and release hydroxyl groups, which also participate in the reaction and improve the catalyst performance [64].

### 3.1.4. Composite metal

All catalysts are affected by the forces of the molecules or atoms, lead to the SMSI are different. These different interactions directly lead to differences in the final activity of the catalyst. Based on this result, scholars have begun to explore the use of two or more active metals as active components of catalysts.

At present, composite metal catalysts typically use noble metals and cheap metals as active components [65,66]. Researchers have hypothesized that the addition of noble metals can increase the low-temperature catalytic performance of the catalyst and that the addition of cheap metals can improve the $N_2$ selectivity of the catalyst.

In general, composite metal catalysts perform better than single metal catalysts. Li *et al.* simultaneously loaded La, Fe, and Pt onto $Al_2O_3$ [67]. The results showed that the mutual doping of noble and cheap metals is better than the catalyst supported by a single metal or by two cheap metals. LaFe-$Al_2O_3$ and LaFePd-$Al_2O_3$ are compared. LaFePd-$Al_2O_3$ showed better acid sites and $NH_3$-SCO activity. This may be because LaFePd-$Al_2O_3$ exhibits an N=N bond length that is lower than the N=N bond length on LaFe during the reaction process when intermediate products containing N=N bonds are formed on both catalysts. From this calculation, it was found that LaFePd-$Al_2O_3$ showed better $NH_3$ affinity. In addition, owing to the addition of Pd, the surface oxygen mobility on the catalyst is reduced, so that the adjacent Fe is rich in more O atoms, and the O density around Fe atoms increases, which makes it easier to generate diazonium (N=N). This also means that the OH bond of -$ON_2H_2$ of intermediate products is easier to break, thereby increasing the selectivity of $N_2$. However, there is no Pd on LaFe-$Al_2O_3$, which leads to -$ON_2H_2$ being mainly dehydrogenated, and thus $N_2$ selectivity is low. According to the experimental results, the research found that the addition of Pd had a certain degree of interaction with the FeO perovskite. Pd and Fe oxides may coexist in the form of Fe-O-Pd. Owing to the influence of Pd-O, the bond energy of Fe-O is correspondingly weakened. Therefore, there is more energy to absorb the transferred oxygen, which makes the Fe-O bond energy of Fe-$ON_2H_2$ stronger. This leads to the weakening of the energy of O-N, so that the N=N energy is strengthened and difficult to break, making the reaction of -$ON_2H_2$ generate intermediate products of $N_2H_2$. The formation of $N_2$ helps to improve the $N_2$ selectivity.

Qu *et al.* loaded Ag, Ce, and Cu on a wire-mesh honeycomb (WMH), and these three metals were combined to form bimetallic composite metal catalysts [68]. Research findings indicate that Ag-WMH has a higher $NH_3$-SCO activity than that of Ag/Cu-WMH, however, Ag/Cu-WMH has higher $N_2$ selectivity. Moreover, compared with Cu-WMH and Cu/Ce-WMH, Ce doping reduces the oxygen bond strength of Cu, leading to a decrease in $N_2$ selectivity. Yu *et al.* found that the addition of Pr to the catalyst enriched the catalyst with more oxygen vacancies [69]. When the reaction gas contains $SO_2$, Pr can inhibit the formation of ammonium sulfate on the catalyst surface, thereby protecting the active metal sites.

The SMSI is related to the manner in which the active material is loaded on the surface of the support [70]. Take Ag supported on the surface of $Al_2O_3$ as an example, Ag loaded on the surface of the $Al_2O_3$, anchored at the O of hydroxyl hydrogen on the surface of the support rather than the O vacancy. Among the terminal hydroxyls, doubly bridging hydroxyls, and triply bridging hydroxyls on the surface of the support, the Ag first selects the terminal hydroxyl groups for anchoring. When the Ag load is small, each active metal atom is anchored to the hydroxyl oxygen to form Ag-(OH)-Al [52]. When more Ag atoms are loaded and the terminal hydroxyls on the surface of the support are insufficient to anchored Ag, that are not anchored to the terminal hydroxyls accumulate on the surface of the support in the form of metal state or clusters, thus greatly reducing the dispersibility of active metals.

Therefore, the terminal hydroxyls on the surface of the support determine the dispersibility of the active metal on the surface of the support and the SMSI, which leads to the difference in catalytic performance caused by different supports loaded with different metals. In addition, the terminal hydroxyl, doubly bridging hydroxyls and triply bridging hydroxyls on the surface of the support also have a certain adsorption capacity for $NH_3$, so that more $NH_3$ can participate in the oxidation reaction on the surface of the support.

At present, the hydroxyl abundance of common supports is arranged in the following order: $Al_2O_3$ > $ZrO_2$ > $TiO_2$ > zeolites [46,71–73]. Notably, zeolite is not a single metal oxide; therefore, its interaction with active metals is also more complicated, and the performance of the catalyst can be adjusted by changing the ratio of Si to Al in the zeolite [71].

## 3.2. Core-shell catalyst

The core-shell catalyst is a special catalyst that can be used to produce catalysts with different gas resistances according to specific reaction conditions and synthesis methods, and is mainly used for $SO_2$ to cause active metal poisoning in $NH_3$-SCO or $NH_3$-SCR [74–77]. The core-shell structure can also prevent the active site from sintering during high-temperature operation and improve the catalytic performance through the synergy produced mainly at the material interface [78,79]. Core-shell catalysts typically use a very stable metal oxide as the shell structure and an active metal as the core.

Wang *et al.* encapsulated $Ag_{NPs}$ with a hollow zeolite, and the hollow structure of the ZSM-5 zeolite prevented the sintering or leaching of silver particles during $NH_3$ oxidation. [59]. Zeolite membranes can provide good separation performance for $SO_2$. Therefore, $SO_2$ did not diffuse into the hollow structure to poison the $Ag_{NPs}$ and induced excellent $SO_2/H_2O$ resistance without any decrease in activity at 150 °C containing 8 vol% $H_2O$ and 100 ppm $SO_2$ (Figs. 3a-d). Ghosh *et al.* wrapped Pt/$Al_2O_3$ with CuZSM-5. Compared with single Pt/ $Al_2O_3$, the $T_{100}$ of the core-shell catalyst decreased by approximately 100 °C [80]. The core-shell catalyst showed enhanced low-temperature activity at the expense of lower Pt loading, while $NO_x$ production rate was <10%. The presence of a Cu-ZSM-5 shell around the Pt/$Al_2O_3$ core had a positive effect on the Pt-support interaction in the core, resulting in the inhibition and instability of the Pt oxide and ultimately enhancing the intrinsic activity of the shell catalysts (Figs. 3e-i). Zhang *et al.* used $CeO_2$ to wrap CuO, and $NH_3$ and $O_2$ molecules entered the interface through porous channels and participated in $NH_3$-SCO under the synergistic effects of CuO and $CeO_2$ (Fig. 3j) [81]. This core-shell structure takes the Cu-O-Ce structure as the active center, which can promote the synergistic effect between the CuO

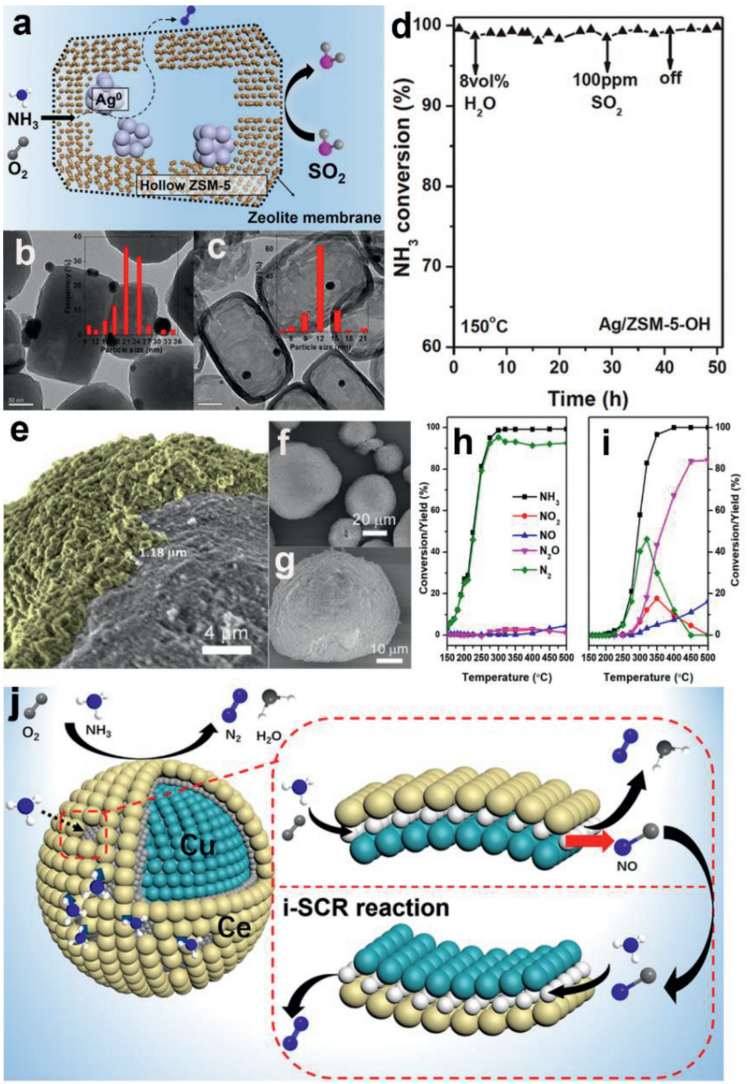


**Fig. 3.** Core-shell materials for $NH_3$-SCO. (a) Reaction mechanism of hollow ZSM-5 supported Ag catalyst, (b) TEM images of ZSM-5 loading Ag, (c) TEM images of hollow ZSM-5 loading Ag, (d) hollow ZSM-5 loading Ag Sulfur resistance and water resistance test. Copied with permission [59]. Copyright 2019, Elsevier. (e-g) SEM of $Pt/Al_2O_3$@Cu/ZSM-5, (h) $Pt/Al_2O_3$@Cu/ZSM-5 active test, (i) $Pt/Al_2O_3$ active test (Reaction conditions: $NH_3 = 500$ ppm, $O_2 = 5$ vol%, GHSV=280,000 $h^{-1}$). Copied with permission [80]. Copyright 2020, Elsevier. (j) Catalyst model of CuO@$CeO_2$ core-shell and reaction path of $NH_3$-SCO.

and $CeO_2$ components and enhance their catalytic performance in $NH_3$-SCO. In addition, this core-shell structure is beneficial to the adsorption and activation of $NH_3$ and to the fixation of NO formed by the i-SCR mechanism, thereby improving the $N_2$ selectivity of the CuO@$CeO_2$ catalyst [81]. Using $SiO_2$ as the shell of the core-shell catalyst can increase the number of Brønsted acid sites in the catalyst without consuming Lewis acid sites [82]. In addition to the $SiO_2$ shell, zeolites can also be used to encapsulate active metals and exhibit good sulfur and water resistance. When comparing the zeolite shell with other shells, ZSM-5 can absorb a large amount of $SO_2$, and its unique pore structure is conducive to $NH_3$ reaction by contact with the active metal [83]. Yang *et al.* found that using $MnO_x$ as the core in the $CeO_x$@X catalyst can increase the pore volume and average pore size of the catalyst, which is beneficial for the adsorption of $NH_3$ [84]. The core-shell structure also has relatively abundant acidic sites [83,85]. This improves the adsorption of $NH_3$ and enhances the $NH_3$-SCO activity of the catalyst at low and high-temperatures. Ghosh *et al.* found that there is a certain degree of interaction between the core and shell [86]. These interactions are beneficial for $NH_3$-SCO and inhibit and destroy the formation of active metal oxides, thereby increasing the activity of the core-shell catalyst. The uniform distribution of the core and shell and the close interaction between them can also generate a large number of Lewis acid sites and enhance the activity of the catalyst [80]. The core-shell of different components will have different interactions, which leads to core-shell catalysts by matching different active cores and highly resistant shell cores; therefore, this catalyst can also be used to improve the activity and $N_2$ selectivity of the reaction by using different composite materials of the core and shell [87,88].

However, the thickness of the shell affects the mass transfer of $NH_3$ to the core, and therefore, also affects the activity of $NH_3$-SCO [89].

## 4. $NH_3$-SCO influencing factor

The performance of $NH_3$-SCO catalysts is influenced by a number of factors. The active center content determines the catalyst performance, while $O_2$, $H_2O$, and $SO_2$ during the reaction process all affect the catalyst activity and selectivity to some extent. Among them, $H_2O$ will severely reduce the catalyst activity, while

$SO_2$ will relatively improve the $N_2$ selectivity while reducing the catalyst activity.

It is well known that the excess of the active metal being loaded will lead to the loss of the overall specific surface area of the catalyst due to the blockage of the pores, so it is not that the more they can be loaded, the better. In addition, the difference of active metal loading may cause the change of active central valence state and particle size (see Supporting information part 1.1). Under practical conditions, $H_2O$ and $O_2$ compete with $NH_3$ for adsorption at the active center site. Both $O_2$ and $NH_3$ need to be activated as major reaction participants, so the concentration or partial pressure of $NH_3/O_2$ affects the conversion of $NH_3$ and $N_2$ selectively at a limited number of active center sites (see Supporting information part 1.2). However, $H_2O$ only hinders the active central site adsorption to $NH_3$ causing the conversion rate of $NH_3$ reduce (see Supporting information part 1.3). $SO_2$ is also one of the factors affecting conversion of $NH_3$. Usually, the active metal site that is vulcanized after high temperature reaction will lose some activity. However, sulfate will participate in $NH_3$-SCO as a reactant and limit the decomposition of intermediate product -HNO, thus improving the selectivity of $N_2$ of the catalyst (see Supporting information part 1.4).

## 5. Reaction mechanism

### 5.1. Research methods of reaction mechanism

Exploring the reaction mechanism of $NH_3$-SCO on different catalysts is a necessary way to reveal the structure-activity relationship of catalysts and guide catalyst design and optimization. A variety of methods have been developed to explore the $NH_3$-SCO reaction mechanism, such as *in situ* DRIFTS, Raman, TPD and DFT (density functional theory) calculations [56,90].

*In situ* DRIFTS is widely used in the mechanism research of various redox reactions. It can observe the intermediate products produced on the surface of the catalyst, which can help the research institute to judge the reaction path (see Supporting information part 2.11). While DRIFTS has a sensitive response time to changes in catalyst surface reactions, it can not resolve nonpolar molecules. Raman can make up for these shortcomings and further analyze the reaction mechanism (see Supporting information part 2.12). In addition, the characterization experiment also needs theoretical verification, so the accuracy of the experiment can be improved through DFT, and the method of exploring the reaction mechanism through the combination of experiment and DFT has been widely accepted by many scholars (see Supporting information part 2.13). It is worth mentioning that the research method of the reaction mechanism is not unique, because the surface acid sites and redox properties of the catalyst may affect the reaction path of $NH_3$, through reference product analysis and various characterization data such as $NH_3$-TPD, $H_2$-TPR, XPS or TEM, are more conducive to the study of $NH_3$-SCO reaction mechanism (see Supporting information part 2.14).

### 5.2. Summary of common $NH_3$-SCO mechanisms

$NH_3$-SCO reaction mechanisms on different catalysts have been widely investigated. The general reaction equation is shown in Eq. 1.

$$2NH_3 + 1.5O_2 = N_2 + 3H_2O \quad (1)$$

Many researchers have put forth different views regarding the specific reaction pathways. To date, four major reaction pathways referred to as the imide (-NH) mechanism [62], i-SCR mechanism (internal selective catalytic reduction mechanism) [91], -$N_4H_4$ mechanism (hydrazine mechanism) [62] and $N_2^-$ mechanism [51], with HNO, $N_2H_4$, $N_2^-$ and SCR-related species as specific intermediates, respectively, have been proposed (For a detailed reaction mechanism, please refer to Supporting information part 2.2).

## 6. Catalyst structure-activity relationship

### 6.1. Valence state of active metal

In $NH_3$-SCO catalysts, studies have shown that active metals are the key factors affecting the catalyst activity. The loading of different metals directly affects the final activity and reaction mechanism of the catalyst. The state of the loaded active metal determines the catalytic activity of the catalyst. It is generally believed that the active metal supported on the support can be divided into three states: aggregated metal oxides, metal element aggregates, and non-aggregated metal oxides formed by combining a single metal atom with oxygen (monoatomic) [34,64,91,92].

We prepared a catalyst that uses nano-$Al_2O_3$ as the support, loaded with 10 wt% of each metal element, and used $H_2$ to reduce the active metal oxide on the support to attempt to make the active metal component exist as elemental. Among the active metals loaded on the support, the catalyst after $H_2$ reduction had higher $NH_3$-SCO activity than before reduction (Fig. 4a). The results showed that the $NH_3$-SCO activity of the M/nano-$Al_2O_3$ catalysts increased significantly after reduction. Therefore, we believe that the activity of the metal element is better than that of the metal oxide in the $NH_3$-SCO process. This finding was confirmed in our previous study [34]. Notably, the catalytic activity of metal oxides does not correspond to the simple substance of the active metal. Before the catalyst is reduced, it can be seen that the catalyst activity is arranged in the following order: $Ag/Al_2O_3 > Cu/Al_2O_3 > Co/Al_2O_3 > Fe/Al_2O_3 > Ni/Al_2O_3$. Because of the large amount of active metal loaded on the support, it can be considered that each active metal aggregates into nanoparticles. The surfaces of these metal nanoparticles are easily oxidized and play a major role in $NH_3$-SCO reactions [63,64,92]. After reduction, the activity of the catalyst increased significantly, and, after $H_2$ reduction, some of the catalysts that were inactive or had low activity before reduction exceeded the activity of the catalysts with medium activity before reduction.

Among the agglomerated metal oxides, $Cu_xO_y$ and $Ce_xO_y$ exhibited excellent redox activity. In all catalysts loaded with Cu, Cu elements were present in the support in the form of $Cu^+$ and $Cu^{2+}$, and these catalysts were in a reducing atmosphere ($NH_3$), and some of the $Cu^{2+}$ was easily reduced to $Cu^+$ [93,94]. $Cu^+$ was oxidized to $Cu^{2+}$ in an oxidizing atmosphere (NO and $O_2$). Next, the transition from $Cu^+$ to $Cu^{2+}$ caused the loss of lattice oxygen during the secondary reduction process, which greatly increased the oxygen vacancies on $Cu_xO_y$. When oxygen vacancies adsorb $O_2$ in the reaction gas, it leads to the production of $Cu^{2+}$ superoxide species; the mechanism of formation of Cu superoxide species is shown in Fig. 4b [95]. The continuous production of superoxide species causes the adsorption and desorption of $O_2$, leading to $O_2$ switching between adsorbed oxygen and lattice oxygen. Thus, $Cu_xO_y$ has a high oxygen-storage capacity. This led to a transition metal Cu oxide with higher $NH_3$-SCO activity. In addition, CuO super oxygen species have a stronger $NH_3$ adsorption capacity than the lattice oxygen or surface oxygen of CuO, making it the active center of $NH_3$-SCO at low-temperatures [44].

The mechanism of action of the $Ce_xO_y$ species is similar to that of $Cu_xO_y$. Both $Ce^{3+}$ and $Ce^{4+}$ redox reactions also lead to strong $O_2$ exchange and the adsorption capacity of $Ce_xO_y$ species. It can also generate $CeO_2$ superoxide species during the oxidation of $Ce^{3+}$ to $Ce^{4+}$ to improve the $NH_3$ oxidation activity [96–98]. However, Ce is rarely used as a single active metal to be loaded on other supports because $CeO_2$ has a lower redox capacity and $NH_3$ ad-

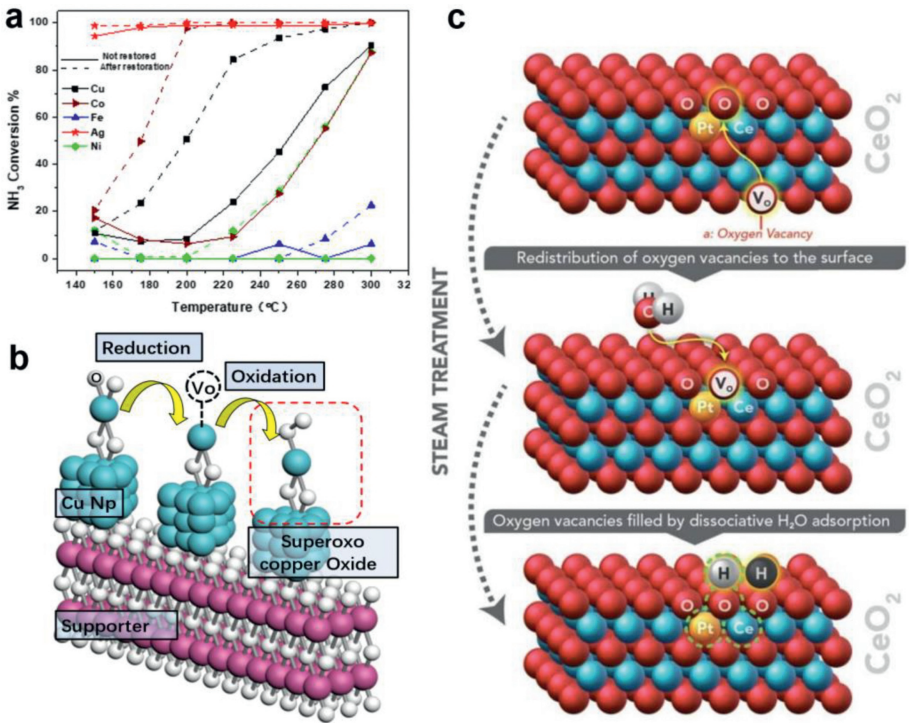


**Fig. 4.** Effects of metal valence state and oxygen type on NH-SCO. (a) Comparison of the activity of each catalyst before and after reduction (Reaction conditions: $NH_3$ 500 ppm, $O_2$ 10%, GHSV = 118,000 $h^{-1}$). (b) Formation mechanism of Cu(II) superoxide species in $CuO_x$. (c) The active site created by the steam treatment over $Pt/CeO_2$. Copied with permission [122]. Copyright 2017, American Association for the Advancement of Science.

sorption capacity [98,99]. Therefore, the degree to which $Ce^{3+}$ and $Ce^{4+}$ can be converted to one another during catalyst synthesis is very important. This also results in ratios of $Ce^{3+}$ to $Ce^{4+}$ in the catalyst, which affects the catalyst activity [100–102]. In addition, the $Ce_xO_y$ species itself does not have strong acid sites to adsorb $NH_3$, which also leads to unsatisfactory catalytic activity of the pure $Ce_xO_y$ species on $NH_3$; therefore, $Ce_xO_y$ cannot be the active component of the $NH_3$-SCO catalyst [52,103]. However, the strong O adsorption capacity of $Ce_xO_y$ itself to load or combine with other metal oxides to become a highly active $NH_3$-SCO catalyst [46,81,104,105].

### 6.2. Oxygen species

Although catalyst activity is typically related to the valence state of the active metal, it ultimately depends on the O activation ability of the active metal or support. There are two types of oxygen species in all catalysts: surface adsorbed oxygen and lattice oxygen. The surface oxygen includes $O_2$, $H_2O$, OH and other structures adsorbed on the catalyst, whereas the lattice oxygen is embedded in the catalyst as part of the catalyst skeleton. The ratio and quantity of lattice oxygen and surface-adsorbed oxygen are factors that affect the final activity of the catalyst [106]. Surface oxygen tends to have higher mobility than lattice oxygen does, and therefore, theoretically, higher $NH_3$ oxidation activity [55,107–109].

The OH group on the catalyst acts as an important source of acidic sites for $NH_3$ adsorption. OH provides protons to $NH_3$ and forms an O-$NH_4$ (Brønsted acid) structure. However, the OH structure, as a weak acid site, does not exhibit a particularly strong $NH_3$ adsorption capacity. It was desorb $NH_3$ from the $Ag/TiO_2$ catalyst at 140 °C [73]. However, the strength of these weaker acid sites can be changed by changing the loaded active metal [110]. After loading Ru species onto $TiO_2$, it was found that the $NH_3$ linked to OH was very stable, and $NH_3$ could be desorbed at 200 °C. The $NH_3$ adsorbed by this O species is completely converted into $N_2$, and the reaction process follows the hydrazine mechanism (Eqs. S20–S22 in Supporting information) [67]. Although the stability of OH-linked $NH_3$ is weak, when the temperature is too high, it is easy to destroy O-$NH_4$ (Brønsted acid site decomposition); however, the hydroxyl group can still dominate the low-temperature $NH_3$-SCO and improve the $N_2$ selectivity [37,81,104,110–113]. This is of great significance in the study of low-temperature $NH_3$-SCO catalysts.

Lattice oxygen as a catalyst framework has a strong ability to link with active metals or supports, and often requires a particularly high-temperature to be reduced and formation O vacancies [111,114–117]. Therefore, the surface oxygen and lattice oxygen cannot be effectively converted at low-temperature, resulting in the catalyst lacking the activation ability of oxygen species [109,118]. Notably, on Ce and Cu oxides, owing to the presence of a certain amount of oxygen vacancies, gaseous O is easily adsorbed to the oxygen vacancies, and is then converted between adsorbed oxygen and lattice oxygen. This results in the release of lattice oxygen and participates in the oxidation of $NH_3$ [65,119]. In this process, when the lattice oxygen is released, the surface oxygen receives the electrons provided by the metal to completely form the metal oxide, and the original oxygen-absorbing site is vacated to form oxygen vacancies [120,121]. In addition, under steam treatment conditions, $H_2O$ molecules can fill the oxygen vacancies on the atomically dispersed $Pt/CeO_2$ surface, generating two adjacent active O lattices near Pt and leading to the formation of Lewis acid-base pairs, thereby promoting $O_2$ activation (Fig. 4c) [122].

Oxygen vacancies strongly adsorb and activate gaseous oxygen, which significantly increases the binding capacity of the catalyst and gaseous oxygen [123]. However, it also leads to the easy formation of superoxide species ($O_2^-$) on Cu and Ce oxides [97]. Because of the gaseous oxygen adsorbed by the oxygen vacancies being activated, O can obtain protons, which in turn increases the number of Brønsted acid sites on the catalyst [123–126]. Notably, the formation of oxygen vacancies is very attractive to O-containing species. Even the by-products formed during the oxi-

dation of $NH_3$ (such as NO) can be supplemented to the oxygen vacancies to break the N=O bond, release N and increase the $N_2$ selectivity of the catalyst [127].

The mutual migration and transformation of the surface oxygen and lattice oxygen play important roles in the catalytic reaction. The formation of superoxide greatly improves the overall activity of the catalyst [122]. However, not all metal oxides can convert their O species between lattice and surface oxygen.

### 6.3. Particle size

#### 6.3.1. Metal clusters and nanoparticles

Generally, the size of the active metal particles also affects the basic performance of the catalyst. When noble metals such as Au, Pt, and Pd are used as active metals, their catalytic activity is correlated with particle size [128]. For the active metal that exists in the state of nanoparticles on the support, the movement and energy states of the extranuclear electron will change with the size of the metal particles. For example, when the size of metal particles decreases, some metal electronic states transition from the metal state to the molecular state. The size of metal nanoparticles determines their crystallographic shape and structure, and the surfaces of metal nanoparticles with different structures can provide different binding structures and strengths, which in turn determine their catalytic activity and selectivity [129].

This is because different crystal surfaces cause differences in atomic structure and electronic state. These differences further lead to different abilities of metal atoms to decompose and adsorb $NH_3$ [130–133]. Among the Pt nanocrystals, Pt (100) had a higher redox activity than that of Pt (111). When the size of the catalyst nanoparticles is reduced to a certain extent, usually a few nanometers or even sub-nanometers, the electronic state and coordination environment of the surface atoms may change dramatically, which will cause the effect of atoms at the corners and edges of the nanoparticles to become dominant [134,135]. An example of the difference in catalyst activity caused by atomic effects is that Pt (557) with a coordination number of 7 has catalytic activity for CO, whereas Pt (557) with a coordination number of 9 has no CO catalytic activity at room temperature [136].

When the size of metal nanoparticles is 1–2 nm, the energy band structure can be expressed as a molecule rather than a metal state, which means that, compared with larger metal particles, the two exhibit completely different catalytic performances [137]. This implies that the electron energy levels associated with metal particles of different sizes are different. The smaller the size, the greater the electron density of the metal particles, the narrower the d orbital, and the closer it is to the Fermi level [138–142]. The closer the electronic energy level is to the Fermi energy level, the higher the energy of the metal atom. In this state, the metal atom usually forms an antibond state, which leads to a stronger interaction between the metal atom and its adsorbate [143–146].

In general, the adsorption energy of active metals is also attributed to the coordination environment of the metal atoms; therefore, it is also believed that the adsorption energy is related to the size of the metal particles. However, this does not mean that the adsorption energy and catalytic activity are higher when the metal particle size is smaller [147]. The activation energy for the chemical adsorption of Pt nanoparticles decreases with decreasing size. In addition, small particles and low-coordination metals are easily bound to certain species so that they are not easily separated from the metal, causing active metal sites to be covered and poisoning of the catalyst [129,148]. At present, cluster catalysts or sub-nanoparticle catalysts have become popular research topics, however, in the field of $NH_3$-SCO, there are few related studies on highly dispersed metal clusters [60]. Larger metal nanoparticles have a higher affinity for the $NH_3$-SCO reaction [35,149,150]. Compared to other macromolecular organics, the $NH_3$-SCO reaction path is relatively simple, and its reaction mainly depends on the activation of $NH_3$ and $O_2$. Notably, cluster catalysts are constructed to strengthen or regulate the interaction between reac-

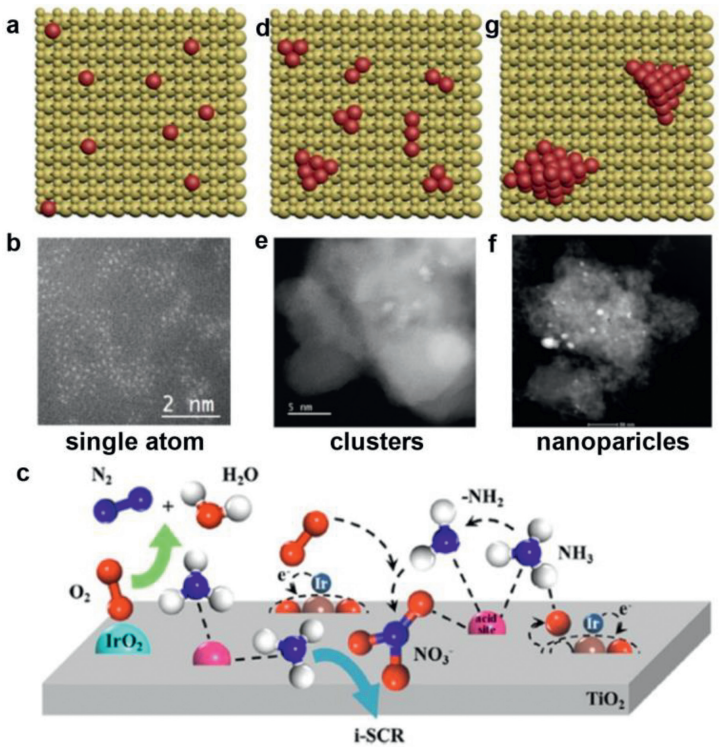


**Fig. 5.** Model and corresponding HADDF-TEM image of single atoms, clusters and nanoparticles. (a-c) Model of single atom, clusters and nanoparticles. (d-f) HADDF-TEM image of single atoms, clusters and nanoparticles. (g) Schematic of the reaction process over $Ir/TiO_2$ catalysts. Copied with permission [26]. Copyright 2022, Elsevier.

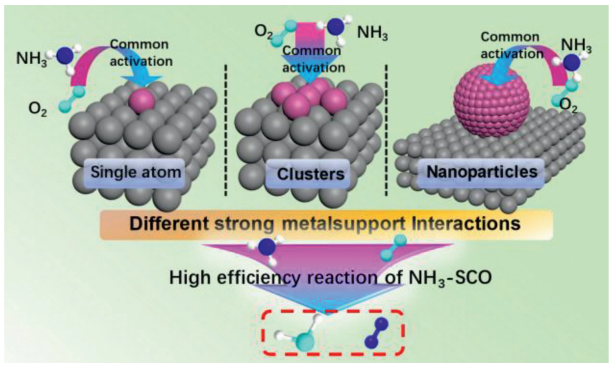


**Fig. 6.** Schematic diagram of high-efficiency $NH_3$-SCO catalyst.

tants and metals and further enhance the selectivity of a product by adjusting the coordination environment of the metal atoms [151–153]. This process is likely to reduce the activation ability of the metal species to $O_2$, therefore, metal nanoparticles with a strong redox ability tend to have better $NH_3$-SCO performance [35,61,117,154,155].

*6.3.2. Single-atom catalysts*

Single-atom catalysts have always been a hot topic in catalyst research. This catalyst disperses the active metal to the extreme so that every atom participates in the catalytic reaction, thus improving catalyst activity. Wang *et al.* synthesized the $Ir_1/TiO_2$ (rutile) catalyst and found that Ir SIMS isolated on the surface of $TiO_2$ (rutile) is stronger than that of $TiO_2$ (anatase) and $TiO_2$ (P25), which results in easier activation of $O_2$ at low-temperatures, thus improving the intrinsic activity of the catalyst [26]. The $T_{100}$ of $Ir_1/Ti$ is at 200 °C and has good water resistance. Currently, research on monatomic catalysts in the field of $NH_3$-SCO is limited. It is difficult to adjust the SMSI perfectly so that $O_2$ and $NH_3$ can be activated efficiently and simultaneously, which makes it difficult to develop monatomic catalysts that can be used in $NH_3$-SCO.

Clusters or nanoparticles formed from single atoms have excellent dispersibility, which can make full use of each active metal atom. The structures of single atoms, clusters, and nanoparticles are shown in Fig. 5. Individual metal elements are usually anchored to metal vacancies, oxygen vacancies, and hydroxyl groups [64,156–158]. Different metals and different supports will form a variety of SMSI, which makes the migration of metal atoms and metal dispersion flexible. According to different conditions, it can make metal atoms agglomerate into fixed-size nanoparticles or atomic clusters [159,160]. This provides a new $NH_3$-SCO research idea using fewer active metals to make the catalyst more active. Even so, research on monatomic catalysts remains promising in the field of $NH_3$-SCO. The coordination environment formed by a single atom is more single, which means that SMSI will be more single, and the exposure of active sites will be greater. In the context of efficient resource utilization, single-atomic catalysts still have great research value. But whether it is designing single-atom, cluster or nanoparticle particle catalysts, the purpose is to improve catalyst performance, $N_2$ selective and reduce costs (Fig. 6).

*6.4. Acid sites*

At present, most researchers have studied the acidic sites on the catalyst surface and the presence of active metals. Most studies have proved the different reaction mechanisms between the Lewis and the Brønsted acid sites, and pointed out that the Brønsted acid site pair $N_2$ selectivity is high. Lewis acid sites have high $NH_3$ oxidation activity and low $N_2$ selectivity [2,46,52,67,161]. Almost all catalysts showed that the richness of Lewis acid sites was considerably greater than that of Brønsted acid sites. In essence, it is difficult to increase the number of Brønsted or Lewis acid sites. Lewis acid sites are usually borne by metal atoms that provide electron pairs. Brønsted acid sites are usually formed by protons provided by hydroxyl groups on the catalyst. The anchoring of the active metal itself is achieved by substituting the hydroxyl hydrogen, so that the more active metal (Lewis acid site) is loaded, the more the hydroxyl group (Brønsted acid site) that can adsorb $NH_3$ decreases. In contrast, when the number of hydroxyl groups is increased, the effective loading of active metals decreases [64]. However, it is easy to strengthen the acid sites on supports loaded with active metals. In our previous study, after using $H_2$ to reduce the $Ag\text{-}Al_2O_3$ catalyst, the acid sites before and after reduction were significantly different [34]. Ag is anchored to $Al_2O_3$ *via* the substituted hydrogen of the terminal hydroxyl group on $Al_2O_3$ with an Ag-O bond, therefore, it occupies the Brønsted acid site on $Al_2O_3$, and $Ag^+$ in the Ag-O bond acts as a new Lewis acid site to adsorb $NH_3$. $H_2$ reduction breaks the Ag-O bond and restores Brønsted acid sites. Ag aggregates with small particles re-expose Lewis acid sites on the covered support. Therefore, for the same support, the larger the specific surface area of the support, the more abundant the acidic sites and other sites are. A schematic of the acid site changes on the $Ag/Al_2O_3$ catalyst before and after $H_2$ reduction is shown in Fig. 7.

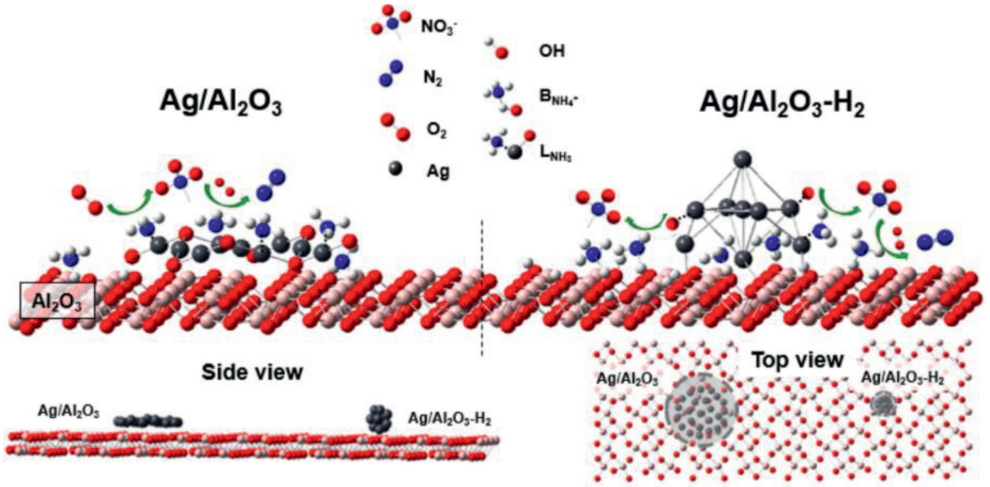


**Fig. 7.** Diagram showing the possible $NH_3$−SCO reaction process over $Ag/Al_2O_3$ and $Ag/\ Al_2O_3-H_2$ (after $Ag/Al_2O_3$ is reduced by $H_2$). Insets are side view and top view of $Ag/\ Al_2O_3$and $Al_2O_3$. Copied with permission [34]. Copyright 2019, American Chemical Society.

**Table 1**
Performance comparison of various catalysts.

| Type | Order | Type of active center | Catalyst code | $T_{50}/T_{100}$ (°C) | $N_2$ selectivity (%) | Reaction condition | Ref. |
|---|---|---|---|---|---|---|---|
| Supported catalyst | 1 | Precious metals | 10%Ag/$Al_2O_3$-$H_2$ | 100/130 | 90/80 | GHSV = 28,000 $h^{-1}$, 500 ppm $NH_3$ | [34] |
| | 2 | | 10%Ag/nano $Al_2O_3$ | 80/140 | 60/70 | GHSV = 136,000 $h^{-1}$, 500 ppm $NH_3$ | [57] |
| | 3 | | 10%Ag/micro $Al_2O_3$ | 140/180 | 95/93 | GHSV = 136,000 $h^{-1}$, 500 ppm $NH_3$ | [57] |
| | 4 | | 1%Pt/ $Al_2O_3$ | 231/300 | 45/30 | GHSV = 100,000 $h^{-1}$, 200 ppm $NH_3$ | [46] |
| | 5 | | 1%Pt/$CeZrO_2$ | 275/- | 62/- | GHSV = 100,000 $h^{-1}$, 200 ppm $NH_3$ | [46] |
| | 6 | | 8%Ag/SiTi | 110/130 | 100/60 | GHSV = 29,000 $h^{-1}$, 500 ppm $NH_3$ | [73] |
| | 7 | | 8%Ag/$TiO_2$ | 160/200 | 100/95 | GHSV = 29,000 $h^{-1}$, 500 ppm $NH_3$ | [73] |
| | 8 | | 10%Ag/ZSM-5 | 90/125 | 77/85 | GHSV = 35,000 $h^{-1}$, 1000 ppm $NH_3$ | [59] |
| | 9 | | 10%Ag/ZSM-OH (hollow zeolite) | 125/150 | 85/88 | GHSV = 35,000 $h^{-1}$, 1000 ppm $NH_3$ | [59] |
| | 10 | Cheap metal | 9.4%Cu-TH-6%-N-400 | 200/300 | 80/98 | GHSV = 100,000 $h^{-1}$, 500 ppm $NH_3$ | [44] |
| | 11 | | 6%Cu@SAPO | 375/- | 85/- | GHSV = 100,000 $h^{-1}$, 500 ppm $NH_3$ | [44] |
| | 12 | | 12%$MoO_3/SiO_2$ | 500/350 | 80/95 | WHSV = 56,250 $h^{-1}$, 960 ppm $NH_3$ | [36] |
| | 13 | | 10%CuOx/H-SSZ-13 | -/250 | -/100 | WHSV = 300,000 $h^{-1}$, 400 ppm $NH_3$ | [72] |
| | 14 | | 10%CuOx/H-SAPO-34 | 250/350 | 100/100 | WHSV = 300,000 $h^{-1}$, 400 ppm $NH_3$ | [72] |
| | 15 | | 2.2%Fe/beta | 375/400 | 40/100 | GHSV = 50,000 $h^{-1}$, 650 ppm $NH_3$ | [2] |
| | 16 | | 1.7%Fe/ZSM-5 | 400/450 | 40/100 | GHSV = 50,000 $h^{-1}$, 650 ppm $NH_3$ | [2] |
| | 17 | | 8.37%CuO/Cu-SSZ-13-O-H | 175/250 | 95/98 | GHSV = 160,000 $h^{-1}$, 500 ppm $NH_3$ | [37] |
| Core-shell catalyst | 18 | | CuO@$CeO_2$-8 (Ce/Cu = 36.6) | 220//240 | 95%/90% | GHSV = 45,000 $h^{-1}$, 1000 ppm $NH_3$ | [81] |
| | 19 | | 10%Cu/ZSM-5@0.05%Pt/$Al_2O_3$ | 250/300 | 50/95 | GHSV = 280,000 $h^{-1}$, 500 ppm $NH_3$ | [80] |
| Composite metal catalyst | 20 | Precious metals | 5%Ag-5%Cu/ $Al_2O_3$ | 210/260 | 79/75 | WHSV = 24,000 $h^{-1}$, 0.5 vol% $NH_3$ | [65] |
| Other metal oxide catalysts | 21 | Cheap metal | CuO-$Fe_2O_3$ (Cu/Fe = 1) | 210/225 | 98/95 | GHSV = 60,000 $h^{-1}$, 800 ppm $NH_3$ | [33] |
| | 22 | | 10%Cu-ATP | 225/440 | 92/83 | GHSV = 15,000 $h^{-1}$, 50 ppm $NH_3$ | [45] |
| | 23 | Precious metals | 2.8wt%Au/$Nb_2O_5$-DO | 110/210 | 100/80 | GHSV = 40,000 $h^{-1}$, 50 ppm $NH_3$ | [2] |
| | 24 | | 1.5%Pt/5%$WO_3/ZrO_2$ | 249/283 | 80/60 | GHSV = 100,000 $h^{-1}$, 180 ppm $NH_3$ | [55] |
| | 25 | | 1.1%Au/$Nb_2O_5$ | 125/250 | 100/90 | GHSV = 30,000 $h^{-1}$, 50 ppm$NH_3$ | [52] |
| | 26 | | 3%Ru-Cu/C | 125/180 | 95/90 | GHSV = 55,000 $h^{-1}$, 50 ppm$NH_3$ | [66] |

In addition, in the current research results, there is a certain amount of water in the application environment of most $NH_3$-SCO catalysts; however, $H_2O$ significantly reduces the performance of the catalyst. Therefore, the impact of $H_2O$ on the catalyst is reduced by the core-shell structure encapsulating the active materials [59,81]. Enhancing the acid sites of the catalyst can also reduce the impact of $H_2O$ on the performance of the catalyst to a certain extent [162].

## 7. Conclusion and perspectives

Ammonia ($NH_3$) has been confirmed to play a crucial role in the formation of haze pollution, and gaseous $NH_3$ can damage the human respiratory tract. Selective catalytic oxidation of $NH_3$ ($NH_3$-SCO) to $N_2$ and $H_2O$ is the most promising purification method. At present, many catalysts with precious metals (such as Pt, Pd, Ru, Ir and Ag) and cheap metals (including Cu, Fe, Mn and Mo, *etc.*) as active centers have been developed. Generally, the $NH_3$ catalyst activity and $N_2$ selectivity in the $NH_3$-SCO reaction show a "see-saw" relationship. Among them, noble metal catalysts have good low-temperature activity, but relatively poor $N_2$ selectivity; while cheap metals usually show high $N_2$ selectivity, but the temperature window is relatively high.

By summarizing the physicochemical properties, catalytic performance and reaction mechanism of various $NH_3$-SCO catalysts, we intend to reveal the structure-activity relationship of the catalysts. First of all, the type, valence and dispersion of the active center will affect the ability of the catalyst to activate oxygen, which is the direct cause of affecting the performance of $NH_3$-SCO. Secondly, the anchoring effect of hydroxyl groups on non-reducible supports ($Al_2O_3$, $SiO_2$) and the SMSI effect on reducible supports ($TiO_2$, $CeO_2$) affect the anchoring state and dispersibility of active metals and then affect their valence and particle size. These factors ultimately determine the ability of catalyst to activate the reactants, which leads to the $NH_3$-SCO reaction proceeding in different pathways (i-SCR, imide, $N_2^-$ mechanism, *etc.*), thus exhibiting

differences in activity and selectivity. It can be seen that this is the fundamental reason that affects the catalytic performance. In addition, some auxiliary factors can increase the catalyst activity. For example, the abundant acid sites of the catalyst are beneficial to the adsorption and activation of $NH_3$; the increase of oxygen content in reaction atmosphere can improve the oxidation performance of $NH_3$. It is also worth noting that in the actual production process, the tail gas is usually accompanied by impurities such as $H_2O$ and $SO_2$, which will affect the catalytic performance to a certain extent. For example, the competitive adsorption of $H_2O$ with $NH_3$ will inhibit the adsorption and activation of $NH_3$, causing the reaction performance. The $SO_2$ poisons the active metals through the formation of sulfates, thus resulting in the deactivation of the catalyst.

In summary, selecting the appropriate active components and carriers according to the requirements of the reaction conditions, and designing the existence state of the active centers through the regulation of the anchor sites on the surface of the carrier, and then further improving the catalytic performance through the regulation of the surface acid sites, is an efficient route to design high-performance $NH_3$-SCO catalysts. In addition, according to the type and content of impurity gas, the catalyst should be further designed to improve the toxicity resistance of the catalyst, and the high performance catalyst in line with practical application should be developed (Table 1).

## Declaration of competing interest

The authors declare that they have no known competing financial interests or personal relationships that could have appeared to influence the work reported in this paper.

## Acknowledgments

This work was financially supported by the National Natural Science Foundation of China (No. 52000093), Yunnan Fundamental Research Projects (No. 202101BE070001-001), National Engineering Laboratory for Mobile Source Emission Control Technology (No. NELMS2019B03).

## Supplementary materials

Supplementary material associated with this article can be found, in the online version, at doi:10.1016/j.cclet.2023.108432.

## References

[1] S.N. Behera, M. Sharma, V.P. Aneja, R. Balasubramanian, Environ. Sci. Pollut. Res. 20 (2013) 8092–8131.
[2] S. Campisi, S. Palliggiano, A. Gervasini, C. Evangelisti, J. Phys. Chem. C. 123 (2019) 11723–11733.
[3] M.A. Sutton, U. Dragosits, Y.S. Tang, D. Fowler, Atmos. Environ. 34 (2000) 855–869.
[4] C. Perrino, M. Catrambone, A.D.M.D. Bucchianico, I. Allegrini, Atmos. Environ. 36 (2002) 5385–5394.
[5] C.L. Zhang, X.S. Geng, H. Wang, L. Zhou, B.G. Wang, Environ. Pollut. 220 (2017) 963–970.
[6] H. Jarnstrom, K. Saarela, P. Kalliokoski, A.L. Pasanen, Environ. Int. 34 (2008) 420–427.
[7] M.Z. Li, C.J. Weschler, G. Beko, et al., Environ. Sci. Technol. 54 (2020) 5419–5428.
[8] Z. Tao, W. Xu, C. Zhu, et al., Poultry Sci. 98 (2019) 1947–1959.
[9] H. Gaafar, R. Girgis, M. Hussein, F. El-Nemr, Acta Oto-Laryngol. 112 (1992) 339–342.
[10] S.G. McNulty, J.D. Aber, S.D. Newman, For. Ecol. Manag. 84 (1996) 109–121.
[11] D.M. Anderson, J.M. Burkholder, W.P. Cochlan, et al., Harmful Algae 8 (2008) 39–53.
[12] X. Liu, L. Duan, J. Mo, et al., Environ. Pollut. 159 (2011) 2251–2264.
[13] V.P. Aneja, H.H. Rogers, E.P. Stahel, J. Air. Pollut. Control. Assoc. 36 (1986) 1338–1341.
[14] J.N. Galloway, J.D. Aber, J.W. Erisman, et al., Bioscience 53 (2003) 341–356.
[15] J. Liu, Y. Zheng, G. Geng, C. Hong, M. Li, Atmos. Chem. Phy. 20 (2020) 7783–7799.
[16] W. Xu, K. Zheng, L. Meng, X. Liu, E. Hartung, Aerosol Air Qual. Res. 16 (2017) 79–90.
[17] S. Guo, M. Hu, M.L. Zamora, et al., Proc. Natl. Acad. Sci. U. S. A. 111 (2014) 17373–17378.
[18] H. Cheng, Q.Y. Hu, S.R. Lou, et al., Environ. Sci. Technol. 52 (2018) 11223–11231.
[19] M. Huang, J. Xu, S. Cai, X. Liu, C. Hu, Atmos. Pollut. Res. 9 (2017) 146–155.
[20] Y. Liu, J. Liggio, R. Staebler, Atmos. Chem. Phy. 15 (2015) 17449–17490.
[21] X. Qi, S. Zhu, C. Zhu, et al., Sci. Total. Environ. 727 (2020) 138632–138642.
[22] Y.C. Chung, C. Huang, C.H. Liu, H. Bai, J. Air Waste Manage. Assoc. 51 (2001) 163–172.
[23] R. Burch, B.W.L. Southward, J. Catal. 198 (2001) 286–295.
[24] T.L. Huang, K.R. Cliffe, J.M. Macinnes, Environ. Sci. Technol. 34 (2000) 4804–4809.
[25] Y. Wu, C. Luo, Q. Su, Ind. Eng. Chem. Res. 58 (2019) 5054–5063.
[26] Y. Wang, W. Xu, X. Chen, et al., J. Hazard. Mater. 432 (2022) 128670–128682.
[27] Y. Chen, X. Chen, X. Ma, et al., J. Catal. 402 (2021) 10–21.
[28] T. Lan, Y. Zhao, J. Deng, et al., Catal. Sci. Technol. 10 (2020) 5792–5810.
[29] S.J. Tauster, S.C. Fung, R.L. Garten, Chem Info 9 (1978) 170–175.
[30] S.D. Elliott, Langmuir. 26 (2010) 9179–9182.
[31] Y.B. Li, C.B. Zhang, J.Z. Ma, et al., Appl. Catal. B 217 (2017) 560–569.
[32] J.H. Kwak, J. Hu, D. Mei, et al., Science 325 (2009) 1670–1673.
[33] H. Wang, Q. Zhang, T. Zhang, et al., Appl. Surf. Sci. 485 (2019) 81–91.
[34] F. Wang, G. He, B. Zhang, et al., ACS Catal. 9 (2019) 1437–1445.
[35] H. Wang, M. Lin, T. Murayama, et al., ACS Catal. 11 (2021) 8576–8584.
[36] L. Lietti, G. Ramis, G. Busca, et al., Catal. Today 61 (2000) 187–195.
[37] T. Zhang, H. Chang, Y. You, et al., Environ. Sci. Technol. 52 (2018) 4802–4808.
[38] R.Q. Long, R.T. Yang, J. Catal. 201 (2001) 145–152.
[39] R.Q. Long, R.T. Yang, Catal. Lett. 78 (2002) 353–357.
[40] G. Jiang, F. Zhang, Z. Wei, et al., Catal. Sci. Technol. 10 (2020) 1477–1491.
[41] D. Macina, A. Opioła, M. Rutkowska, et al., Mater. Chem. Phy. 187 (2017) 60–71.
[42] H. Wang, R. Zhang, Y. Liu, et al., Environ. Sci. Nano. 7 (2020) 1399–1414.
[43] M. Jabłońska, ChemCatChem 12 (2020) 4490–4500.
[44] F. Han, M. Yuan, S. Mine, et al., ACS Catal. 9 (2019) 10398–10408.
[45] C. Chen, Y. Cao, S. Liu, et al., Appl. Surf. Sci. 480 (2019) 537–547.
[46] M. Sun, J. Liu, C. Song, Y. Ogata, H. Rao, ACS Appl. Mat. Int. 11 (2019) 23102–23111.
[47] C.M. Hung, Powder Technol. 200 (2010) 78–83.
[48] R.Q. Long, R.T. Yang, Catal. Lett. 78 (2002) 353–357.
[49] C.M. Hung, J. Hazard. Toxic. Radio. Waste. 15 (2011) 37–41.
[50] J.H. Shin, G.J. Kim, S.C. Hong, Appl. Surf.e Sci. 506 (2020) 144906.
[51] M. Sun, S. Wang, Y. Li, et al., J. Taiwan Inst. Chem. E 78 (2017) 401–408.
[52] M. Lin, B. An, N. Niimi, ACS Catal. 9 (2019) 1753–1756.
[53] Z. Zhang, Y. Zhu, H. Asakura, et al., Nat. Commun. 8 (2017) 16100.
[54] S. Ding, H.A. Chen, O. Mekasuwandumrong, et al., Appl. Catal. B 281 (2021) 119471–119481.
[55] M. Sun, S. Wang, Y. Li, et al., Appl. Surf. Sci. 402 (2017) 323–329.
[56] M. Lin, B. An, T. Takei, et al., J. Catal. 389 (2020) 366–374.
[57] F. Wang, J. Ma, G. He, et al., ACS Catal. 8 (2018) 2670–2682.
[58] L. Gang, B.G. Anderson, J. van Grondelle, et al., J. Catal. 206 (2002) 60–70.
[59] Z. Wang, Q. Sun, D. Wang, et al., Sep. Purif. Technol. 209 (2019) 1016–1026.
[60] C.W. Lopes, J. Martinez-Ortigosa, K. Góra-Marek, et al., J. Mat. Chem. A 9 (2021) 27448–27458.
[61] G. Xu, Y. Zhang, J. Lin, Y. Wang, X. Shi, ACS Catal. 11 (2021) 5506–5516.
[62] L. Zhang, H. He, J. Catal. 268 (2009) 18–25.
[63] Z. Qu, H. Wang, S. Wang, et al., Appl. Surf. Sci. 316 (2014) 373–379.
[64] F. Wang, J. Ma, S. Xin, et al., Nat. Commun. 11 (2020) 529–538.
[65] M. Jabłońska, K. Nothdurft, M. Nocuń, V. Girman, et al., Appl. Catal. B 207 (2017) 385–396.
[66] J. Fu, K. Yang, C. Ma, et al., Appl. Catal. B 184 (2016) 216–222.
[67] P. Li, R. Zhang, N. Liu, S. Royer, Appl. Catal. B 203 (2017) 174–188.
[68] Z. Qu, Z. Wang, X. Quan, et al., Chem. Eng. J. 233 (2013) 233–241.
[69] C.L. Yu, B.C. Huang, L.F. Dong, et al., Chem. Eng. J. 316 (2017) 1059–1068.
[70] H. KnoZinger, P. Ratnasamy, Catal. Rev. 17 (2007) 31–70.
[71] J. Guo, W. Yang, Y. Zhang, et al., Catal. Commun. 135 (2020) 105751–105756.
[72] J. Guo, Y. Peng, Y. Zhang, et al., Appl. Catal. A 585 (2019) 117119–117127.
[73] F. Wang, J. Ma, G. He, et al., Ind. Eng. Chem. Res. 52 (2018) 11903–11910.
[74] R. Ghosh Chaudhuri, S. Paria, Chem. Rev. 112 (2011) 2373–2433.
[75] J.D. Rimer, A. Chawla, T.T. Le, Annu. Rev. Chem. Biomol. 9 (2018) 283–309.
[76] A. Ghorbanpour, A. Gumidyala, L.C. Grabow, et al., ACS Nano 9 (2015) 4006–4016.
[77] S.T. Hunt, M. Milina, A.C. Alba-Rubio, et al., Science 352 (2016) 974–978.
[78] J.A.S. Das, N.D.Z. Bian, M.H. Wai, et al., Appl. Catal. B 230 (2018) 220–236.
[79] L. Zhang, D. Jianping, S. Cai, et al., Nanoscale 5 (2013) 9821–9829.
[80] R.S. Ghosh, T.T. Le, T. Terlier, et al., ACS Catal. 10 (2020) 3604–3617.
[81] X. Zhang, H. Wang, X. Jiang, et al., Catal. Sci. Technol. 9 (2019) 2968–2981.
[82] C. Liu, L. Chen, J. Li, et al., Environ. Sci. Technol. 46 (2012) 6182–6189.
[83] R. Yan, S. Lin, Y. Li, et al., J. Haz. Mat. 396 (2020) 122592–122603.
[84] C. Yang, J. Yang, Q. Jiao, D. Zhao, Ceram. Int. 46 (2019) 4394–4401.
[85] S. Liu, H. Wang, Y. Wei, R. Zhang, Mol. Catal. 485 (2020) 110822–110834.
[86] S. Cheng, J. Shao, B. Huang, et al., RSC Adv. 10 (2020) 13855–13865.
[87] J. Pu, K. Nishikado, N. Wang, et al., Appl. Catal. B 224 (2017) 69–79.
[88] W. Ding, M. Klumpp, S. Lee, Chem. Ing. Tech. 87 (2015) 702–712.

[89] S. Shrestha, M.P. Harold, K. Kamasamudram, et al., Catal. Today 267 (2016) 130–144.
[90] D. Song, X. Shao, M. Yuan, et al., RSC Adv. 6 (2016) 88117–88125.
[91] M. Amblard, R. Burch, B.W.L. Southward, Catal. Today 59 (2000) 365–371.
[92] M. Jabłońska, R. Palkovits, Appl. Catal. B 181 (2016) 332–351.
[93] E. Borfecchia, M. Dyballa, I.A. Pankin, et al., J. Am. Chem. Soc. 139 (2017) 14961–14975.
[94] R. Martínez-Franco, M. Moliner, P. Concepcion, et al., J Catal. 314 (2014) 73–82.
[95] J. Sárkány, J. Mol. Struct. 410 (1997) 95–98.
[96] V.K. Paidi, L. Savereide, D.J. Childers, et al., ACS Appl. Mat. Int. 9 (2017) 30670–30678.
[97] J. Xu, J. Harmer, G. Li, T. Chapman, et al., Chem. Commun. 46 (2010) 1887–1889.
[98] X.F. Tong, T. Luo, X. Meng, et al., Small 11 (2015) 5581–5588.
[99] Lykaki, Maria, Pachatouridou, et al., Appl. Catal. B 230 (2018) 18–28.
[100] R. Wang, C. Chen, S.J. Deng, et al., J. Chil. Chem. Soc. 59 (2014) 2710–2716.
[101] J.S. Elias, M. Risch, L. Giordano, et al., J. Am. Chem. Soc. 136 (2014) 17193–17200.
[102] P. Hartmann, T. Brezesinski, J. Sann, et al., ACS Nano 7 (2013) 2999–3013.
[103] S.H. Kim, B.C. Park, Y.S. Jeon, et al., ACS Appl. Mat. Int. 10 (2018) 32112–32119.
[104] Z. Wang, Z. Qu, X. Quan, Z. Li, H. Wang, Appl. Catal. B 134-135 (2013) 153–166.
[105] A. Jha, D.W. Jeong, Y.L. Lee, et al., RSC Adv. 5 (2015) 103023–103029.
[106] K. Min, E.D. Park, M.K. Ji, J.E. Yie, Appl. Catal. A 327 (2007) 261–269.
[107] Z. Qu, Z. Wang, X. Zhang, H. Wang, Catal. Sci. Technol. 6 (2016) 4491–4502.
[108] Z. Qu, R. Fan, Z. Wang, H, et al., Appl. Surf. Sci. 351 (2015) 573–579.
[109] Z. Wu, R. Jin, Y. Liu, H. Wang, Catal. Commum. 9 (2008) 2217–2220.
[110] Q. Zhang, T. Zhang, F. Xia, et al., Appl. Surf. Sci. 500 (2020) 144044–144055.
[111] W. Yue, R. Zhang, N. Liu, B. Chen, Chin. Sci. Bull. 59 (2014) 3980–3986.
[112] Z. Wang, Z. Qu, X. Quan, H. Wang, Appl. Catal. A 411-412 (2012) 131–138.
[113] Z. Wang, Z. Qu, R. Fan, Sep. Purif. Technol. 147 (2015) 24–31.
[114] M. Amblard, R. Burch, B.W.L. Southward, Appl. Catal. B 22 (1999) 159–166.
[115] C. Chen, Y. Cao, S. Liu, W. Jia, Appl. Surf. Sci. 507 (2020) 145153–145161.
[116] L. Chmielarz, A. Węgrzyn, M. Wojciechowska, et al., Catal. Lett. 141 (2011) 1345–1354.
[117] L. Gang, B.G. Anderson, J. van Grondelle, R.A. van Santen, Appl. Catal. B 40 (2003) 101–110.
[118] H. Chen, A. Sayari, A. Adnot, F. Larachi, Appl. Catal. B 32 (2001) 195–204.
[119] Z. Yang, T.K. Woo, M. Baudin, K. Hermansson, J. Chem. Phys. 120 (2004) 7741–7749.
[120] J.H. Lunsford, Adv. Catal. 22 (1972) 265–344.
[121] M. Che, A.J. Tench, Adv. Catal. 32 (1983) 1–148.
[122] L. Nie, D. Mei, H. Xiong, Science 358 (2017) 1491–1523.
[123] F. Liu, H. He, Y. Ding, C. Zhang, Appl. Catal. B 93 (2009) 194–204.
[124] L. Chengyin, Z. Yihe, P. Nicola, et al., Appl. Catal. B 203 (2017) 465–474.
[125] R.Q. Long, R.T. Yang, J. Catal. 190 (2000) 22–31.
[126] A. Khan, P.G. Smirniotis, J. Mol. Catal. A Chem. 280 (2008) 43–51.
[127] W. Yang, M. Liang, Acta Phy. Sin.Chinese. Ed. 54 (2005) 2207–2211.
[128] M.S. Chen, D.W. Goodman, Catal. Today 111 (2006) 22–33.
[129] S. Cao, F.F. Tao, Y. Tang, et al., Chem. Soc. Rev. 45 (2016) 4747–4765.
[130] H. Zhang, M. Jin, Y. Xiong, et al., Acc. Chem. Res. 46 (2013) 1783–1794.
[131] R. Narayanan, M.A. El-Sayed, J. Phy. Chem. B 109 (2005) 12663–12676.
[132] J. Chen, B. Lim, E.P. Lee, Y. Xia, Nano Today 4 (2009) 81–95.
[133] C. Wang, H. Daimon, T. Onodera, et al., Angew. Chem. Int. Ed. 120 (2008) 3644–3647.
[134] G.A. Somorjai, R.M. Rioux, Catal. Today 100 (2005) 201–215.
[135] M. Che, C.O. Bennett, D.D. Eley, H. Pines, P.B Weisz, The influence of particle size on the catalytic properties of supported metals, Adv. Catal., Academic Press, 1989, pp. 55–172.
[136] F. Tao, S. Dag, L.W. Wang, et al., Science 327 (2010) 850–853.
[137] C.L. Cleveland, U. Landman, T.G. Schaaff, et al., Phys. Rev. Lett. 79 (1997) 1873–1876.
[138] M. Chen, D.W. Goodman, Chem. Soc. Rev. 37 (2008) 1860–1870.
[139] M.S. Chen, D.W. Goodman, Science 306 (2004) 252–255.
[140] J.A. Vanbokhoven, J.T. Miller, J. Phy. Chem. C 111 (2007) 9245–9249.
[141] T.V.W. Janssens, A. Carlsson, A. Puig-Molina, B.S. Clausen, J. Catal. 240 (2006) 108–113.
[142] M.J. Walsh, K. Yoshida, A. Kuwabara, et al., Nano Lett. 12 (2012) 2027–2031.
[143] B. Hammer, J.K. Norskov, Nature 376 (1995) 238–240.
[144] B. Hammer, O.H. Nielsen, J.K. Nrskov, Catal. Lett. 46 (1997) 31–35.
[145] J. Nrskov, T. Bligaard, B. Hvolbk, et al., Cheminform 37 (2008) 2163–2171.
[146] J.K. Nørskov, T. Bligaard, J. Rossmeisl, C.H. Christensen, Nat. Chem. 1 (2009) 37–46.
[147] H.M. Lu, X.K. Meng, J. Phys. Chem. C 114 (2010) 1534–1538.
[148] U. Heiz, A. Sanchez, S. Abbet, W.D. Schneider, J. Am. Chem. Soc. 121 (1999) 3214–3217.
[149] J. Martinez-Ortigosa, C.W. Lopes, G. Agostini, et al., Micropor. Mesopor. Mat. 323 (2021) 111230–111243.
[150] M. Sun, S. Zhou, S. Wang, C. Song, ACS Omega 7 (2022) 3177–3184.
[151] Y. Tang, V. Fung, X. Zhang, Y. Li, L. Nguyen, J. Am. Chem. Soc. 143 (2021) 16566–16579.
[152] X. Han, X. Ling, Y. Wan, et al., Angew. Chem. Int. Ed. 58 (2019) 5359–5364.
[153] Y. Zhang, S. Wu, Y. Li, et al., ACS Appl. Nano Mater. 4 (2021) 9866–9875.
[154] G. Xu, H. Wang, Y. Yu, H. He, J. Catal. 395 (2021) 1–9.
[155] B. Qiao, J. Liu, Y.G. Wang, Q.Q. Lin, X. Liu, ACS Catal. 5 (2015) 6249–6254.
[156] Y. Chen, S. Ji, W. Sun, et al., Angew. Chem. Int. Ed. 59 (2020) 1295–1301.
[157] H. Guan, J. Lin, B. Qiao, S. Miao, A.Q. Wang, AIChE J. 63 (2017) 2081–2088.
[158] S.C. Ammal, A. Heyden, Chem. Ing. Tech. 89 (2017) 1343–1349.
[159] T.W. Hansen, A.T. Delariva, S.R. Challa, A.K. Datye, Acc. Chem. Res. 46 (2013) 1720–1730.
[160] R. Lang, X. Du, Y. Huang, et al., Chem Rev. 120 (2020) 11986–12043.
[161] G. Ramis, L. Yi, G. Busca, Catal. Today 28 (1996) 373–380.
[162] S.M. Jeong, S.H. Jung, K.S. Yoo, S.D. Kim, Ind. Eng. Chem. Res. 38 (1999) 2210–2215.